AMERICAN SCIENTIFIC PUBLISHERS

Science of Advanced Materials
Vol. 11, pp. 699–707, 2019
www.aspbs.com/sam

ARTICLE

Optimization of Epoxypinane Synthesis by Silicotungstic Acid Supported on SBA-15 Catalyst Using Response Surface Methodology

Zhengjun Shi[1,2], Chunhua Wu[1,2,*], Yang Wu[3,5], Huiqing Liu[2], Gaofeng Xu[1,2], Jia Deng[1,2], Hongbo Gu[4,*], Hu Liu[5,6], Jiaoxia Zhang[5,7], Ahmad Umar[8,*], Yong Ma[9,*], and Zhanhu Guo[5,*]

[1]*Key Laboratory for Forest Resources Conservation and Utilization in the Southwest Mountains of China, Ministry of Education, Southwest Forestry University, Kunming 650224, P. R. China*
[2]*School of Chemical Engineering, Southwest Forestry University, Kunming 650224, P. R. China*
[3]*School of Materials Science and Engineering, Nanchang University, Nanchang 330031, P. R. China*
[4]*Shanghai Key Lab of Chemical Assessment and Sustainability, Department of Chemistry, Tongji University, Shanghai, 200092, China*
[5]*Integrated Composites Laboratory (ICL), Chemical & Biomolecular Engineering Department, University of Tennessee, Knoxville, TN 37996, USA*
[6]*Key Laboratory of Materials Processing and Mold (Zhengzhou University), Ministry of Education; National Engineering Research Center for Advanced Polymer Processing Technology, Zhengzhou University, Zhengzhou, 450002, China*
[7]*School of Material Science and Engineering, Jiangsu University of Science and Technology, Zhenjiang, Jiangsu, 212003, China*
[8]*Department of Chemistry, Faculty of Sciences and Arts, Promising Centre for Sensors and Electronic Devices (PCSED), Najran University, P.O. Box 1988, Najran, 11001, Saudi Arabia*
[9]*School of Materials Science and Engineering, Shandong University of Science and Technology, Qingdao 266590, China*

ABSTRACT

Silicotungstic acid supported on SBA-15 (SiW_{12}/SBA-15) has been synthesized under hydrothermal conditions and characterized with various analytical and spectroscopic techniques including X-ray diffraction (XRD), N_2 adsorption, transmission electron micrographs (TEM), and Fourier transform infrared spectroscopy (FT-IR). The catalytic activities of SiW_{12}/SBA-15 catalysts were evaluated in the epoxidation of α-pinene. 2,3-epoxypinane was the main product. The results showed that under the optimum conditions with 22.5 wt% loading of silicotungstic acid, 1.8 wt% of catalyst dosage, peracetic acid and α-pinene molar ratio of 1.15, and 2.5 h of reaction time, the yield of 2,3-epoxypinane reached 90.30%. When the SiW_{12}/SBA-15 was recycled for the fourth time, the catalytic efficiency decreased. The conversion rate of α-pinene and the selectivity was 81.65% and 89.44%, respectively.

KEYWORDS: α-Pinene, SBA-15, SiW_{12}/SBA-15, Silicotungstic Acid, Epoxidation.

1. INTRODUCTION

With the continuous development and progress of science and technology, advanced materials with small size, high dimensions, and multi-functional such as ceramics, polymers, composites, semiconductors, and superconductors gradually attracted a wide range of research interests.[1–23] The advanced materials with excellent mechanical, transmission, optical, electrical, magnetic, and thermal properties replaced the traditional materials in biological, energy, medical, aerospace, electric power, polymer industrials, corrosion and protection, and other industrial applications.[24–37] Mesoporous materials with uniform pore structure and an extensively high surface area have been reported for the potential applications of catalysts, adsorbents for large organic molecules and guest-host chemical supports.[38–40] In the family of mesoporous materials, SBA-15 is a newly discovered mesoporous silica molecular sieve with uniform tubular channels and has a variable pore diameter from 50 to 300 Å. Compared with MCM-41, SBA-15 has a larger pore diameter, thicker pore wall and higher hydrothermal stability.[41] SBA-15 materials

*Authors to whom correspondence should be addressed.
Emails: kmwuchunhua@163.com, hongbogu2014@tongji.edu.cn, ahmadumar786@gmail.com, mayongfn@gmail.com, zguo10@utk.edu
Received: 6 June 2018
Accepted: 26 July 2018

modified by different functional groups have been studied, for example, the incorporations of Al,[42–43] Ti,[44–45] Sn[46] or V[47] into SBA-15 has appeared recently. The post-synthesis method is still overwhelmingly used, mainly because SBA-15 needs strong acidic synthesis conditions, and exhibits a great deal of useful characters. There are few papers about the modification and applications of SBA-15 with heteropolyacid.[48–49]

The catalytic epoxidation of alkenes has been a subject of growing interests in the fundamental chemistry and modern industrial processes, since epoxides are key building blocks in organic synthesis.[50–51] α-Pinene is the main component of turpentine. Its double bond with the great reactivity is prone to epoxidation reactions over the acidic catalyst. The epoxidation of alkenes is one of the key steps in functionalizing hydrocarbons and rapidly building functionality into a range of molecules. This is because epoxides are highly useful intermediates for the manufacture of many important commercial products, such as corrosion-protecting agents, pharmaceuticals, additives, etc.[52–53] Their selective synthesis is of considerable academic and industrial interests. The homogeneous catalysts such as peracids have been mostly used in the industrial production of epoxides from the oxidation of alkenes (except for light alkenes). However, this inevitably produces a lot of wastes, polluting the environment. From the view point of sustainable and green chemistry, heterogeneous catalysts would be attractive since they offer the advantages of facile catalyst separation, possible catalyst recycling and high selectivity. Environmental considerations and handling difficulties have led to sustained efforts in recent years to replace homogeneous acid catalysts with solid acid catalysts.

In this study, SBA-15 modified with silicotungstic acid was prepared by post-synthetic methods for the first time to our knowledge. The characterization and catalytic properties of these materials were also illustrated. The transmission electron microscopy (TEM) and powder X-ray diffraction (XRD) results proved that the modification was successful and molecular sieves were not destroyed. The catalytic activities of modified mesoporous silica molecular sieves were evaluated in the epoxidation of α-pinene.

2. EXPERIMENTAL DETAILS

2.1. Materials

Tetraethoxysilane and sodium hyposulfite were purchased from Sinopharm Chemical Reagent Co., Ltd. (China), Pluronic P123 triblockpolymer ($EO_{20}PO_{70}EO_{20}$, Mav = 5800, from Aldrich), silicotungstic acid were purchased from China Pharmaceutical Shanghai Chemical Reagent Company (China). Hydrochloric acid, sulphuric acid and trichloromethane were purchased from Yunnan Yang Lin Industrial Development Zone Shandian Pharmaceutical Co., Ltd. (China). Anhydrous sodium carbonate, anhydrous sodium sulfate, and tetrabutylbromide were provided by Tianjin Zhiyuan Chemical Reagent Co., Ltd. (China). All these reagents were analytical purity grades.

2.2. Synthesis of SBA-15

The catalyst of SBA-15 was prepared according to the reported procedures.[54] Briefly, 9.4 mL tetraethyl orthosilicate (TEOS) was added to 30 mL 0.2 mol/L aqueous HCl solution. This solution was mechanically stirred for 3 h at 313 K and then added into 63 mL 0.2 mol/L aqueous HCl solution containing 4 g P123 ($EO_{20}PO_{20}EO_{20}$, Aldrich). After mechanically stirred for 24 h, this gel was transferred to an autoclave and kept at 373 K for 24 h. Then it was cooled down to room temperature. The solid obtained was filtered off, washed with distilled water to neutrality, dried at 353 K overnight, and heated finally to 823 K at a heating rate of 5 K/min and then maintained for 6 h. The sample was marked as SBA-15.

2.3. Synthesis of SBA-15 Supported Silicotungstic Acid

SBA-15 mesoporous molecular sieve (1 g) and 0.43 g of $H_6O_{41}SiW_{12}$ (SiW_{12}) were added to 20 mL deionized water, mechanically stirred for 5 h, dried at 100 °C for 5 h, and then calcined at 350 °C for 3 h. The sample was indexed as SiW_{12}/SBA-15 (30). SBA-15 mesoporous molecular sieve loaded with 20%, 40% and 50% silicotungstic acid was prepared by the aforementioned method.

2.4. Characterization of SBA-15

XRD patterns were recorded between $2\theta = 0.1{\sim}10.0°$ and $2\theta = 5.0{\sim}80.0°$, respectively, on a Nicolet powder X-ray diffraction apparatus equipped with a Cu-K_α irradiation operating at 40 kV and 100 mA.

Nitrogen adsorption–desorption isotherms were measured with a Tristar 3000 surface area and porosimetry analyzer (Micromeritics Instrument Corp., USA). Brunauer-Emmett-Teller (BET) surface area was determined from the linearity of BET equation. Pore size and its distribution were calculated using desorption isotherm branch and the Barrett-Joyner-Halenda (BJH) formula. The samples were outgassed for 12 h at 383 K in a vacuum (10^{-6} Torr) prior to the measurement.

TEM images were taken on a JEM-2010 TEM instrument with an accelerating voltage of 200 kV to investigate the fine structure, morphology and particle size.

FT-IR spectra were recorded on a Thermoscientific Nicolet 380 FT-IR spectrometer at 2 cm^{-1} resolution using a KBr pellet technique. Before measurement, all samples and KBr were dried in a loft drier at 773 K overnight. The sample diluted in KBr (2.0 wt%) was pressed into a wafer.

2.5. Synthesis of 2,3-Epoxypinane

2,3-Epoxypinane was synthetized by α-pinene and peroxyacetic acid in a flask with a condenser at the reflux

temperature, in the presence of silicotungstic acid supported on SBA-15 (SiW_{12}/SBA-15) as catalyst and quaternary ammonium tetrabutyl ammonium bromide as a phase transfer catalyst. In addition, low reaction temperature was beneficial to the epoxidation, and thus the epoxidation should be conducted below 10 °C. After the reaction, reaction solution was fully mixed with 200 mL water to dissolve CH_3COONa and remove solid by filtration. The liquid was then separated into the water layer and the organic layer in the liquid separation funnel, then extracted the water layer 1 to 2 times with $CHCl_3$, collected the lower liquid and merged with the organic layer. The organic layer was washed with saturated NaCl solution and saturated $Na_2S_2O_3$ solution in turn. The collected lower layer liquid was washed with saturated NaCl solution to neutral. After drying with Na_2SO_4, the product was a colorless, transparent liquid with cool smell. The liquid organic products were quantified using a gas chromatograph (Agilent 7890) with a capillary column (CPB10-S25-050) and a FID detector, in which nitrogen was used as a carrier gas with injected port temperature of 523 K and programmed ramping column temperature from 353 to 523 K (3 K min^{-1}). The diversion ratio was 1:50. The formula of conversion rate is formula (1) and the formula of selectivity is formula (2).

$$\text{Conversion rate } (X)\% = \frac{\text{moles of (initial } \alpha\text{-pinene} - \text{surplus } \alpha\text{-pinene)}}{\text{moles of initial } \alpha\text{-pinene}} \times 100\% \quad (1)$$

$$\text{Selectivity } (S)\% = \frac{\text{moles of 2,3-epoxypinane}}{\text{moles of (initial } \alpha\text{-pinene} - \text{surplus } \alpha\text{-pinene)}} \times 100\% \quad (2)$$

2.6. RSM Design of Epoxidation of α-Pinene by SiW_{12}/SBA-15

The response surface method (RSM) was used to investigate the interaction between factors, and the optimal single factor values. The RSM experimental design was selected for the four factors and three levels, the dosage of the catalyst, peracetic acid and α-pinene molar ratio, and reaction time. The experimental design was shown in Table I.

Table I. Coded values of the variables for the Box-Behnken design.

		Variable levels		
Variables	Symbols	−1	0	1
Loading amount (%)	X_1	20	30	40
Dosage of catalyst (%)	X_2	1.5	2.0	2.5
Molar ratio of peracetic acid to α-pinene	X_3	1.1	1.2	1.3
Reaction time (h)	X_4	2	3	4

3. RESULTS AND DISCUSSION

3.1. XRD Characterization

The XRD patterns of SBA-15 and SiW_{12}/SBA-15 (30) are depicted in Figure 1. The observed intense peak (100) at $2\theta = 0.9°$, an additional peak (110) and a very weak peak (200) in the small angle range are the typical diffraction peaks for SBA-15. The peaks of SBA-15 are located at 0.9°, 1.5° and 1.8°. These prove that the pore of modified materials has a high degree ordering hexagonal structure.[54] This indicates a good mesoscopic order and the characteristic hexagonal features of SBA-15 maintained in SiW_{12} (30)/SBA-15 samples. Silicotungstic acid does not alter the XRD patterns. According to the large angle XRD patterns (2θ = 5–40°), the diffraction patterns are very diffusive. According to the literature, the characteristic peaks of pure silicotungstic acid are 7°∼10°, 15°∼22°, 26°∼31°, 34°∼39°. However, the characteristic peaks of silicotungstic acid in the wide angle X-ray diffraction do not appear, which assume that silicotungstic acid is well dispersed on SBA-15.

3.2. Nitrogen Adsorption–Desorption Isotherms

In the isothermal diagram, a typical irreversible-type IV adsorption isotherm with a hysteresis loop as defined by IUPAC for the SiW_{12}/SBA-15 catalyst is observed. There are two obvious inflection points in the range of 0.60 to 0.90, indicating that the SiW_{12}/SBA-15 catalyst has the same adsorption type as SBA-15, and belongs to the fourth type adsorption–desorption isothermal model. After loading, the N_2 adsorption–desorption curve of sample moves to a relatively small pressure direction, and then begins to move smoothly near 0.9, which is the same as the adsorption isotherm of SBA-15 in the literature.[55] The hysteresis loop is a typical feature of mesoporous materials. An increase in the N_2 adsorption amount due to multilayer adsorption was observed at higher-pressure region as SBA-15 has a larger pore size than MCM-41.[56–57] The average diameters of primary mesopores, labeled as DBJH, were obtained from the maximum of a pore size distribution using the BJH method (Table II). The specific surface area and the average pore size were decreased after silicotungstic acid loading. Siliceous SBA-15 possesses a narrow pore size distribution and a high mesoporous surface area with considerable micropores, as seen from Table I. The impregnation of silicotungstic acid reduced the surface area. The *t*-plot analysis was used to estimate the micropore volume in SBA-15. A gradual disappearance of the micropores on incorporation of silicotungstic acid in SBA-15 was observed. Combining this with the above BET analysis, the observed decrease in the surface area during silicotungstic acid addition is essentially due to the loss of micropores. Since the micropores are probably generated by the penetration of hydrophilic poly(ethylene oxide) chains of triblock copolymer into its thick silica walls, hydrothermal heating would shrink the silica walls to mend the "holes" therein, which are micropores.[58–62]

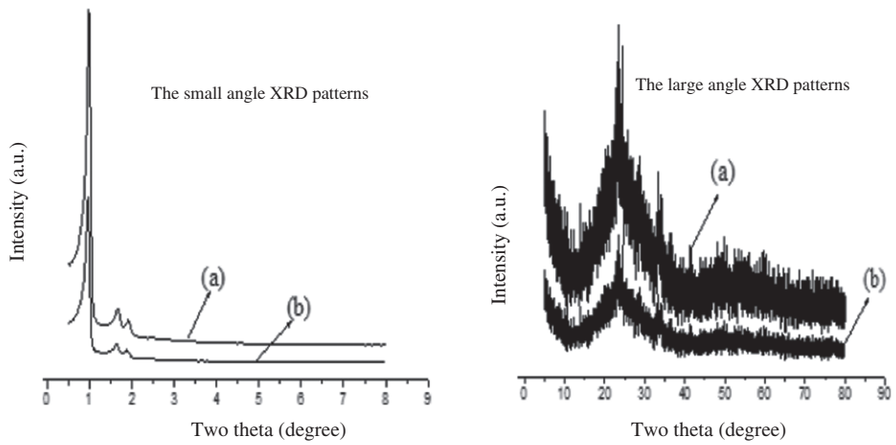

Fig. 1. XRD of SBA-15 (a) and SiW_{12} modified SBA-15 (b).

From Table I, it is seen that with the increase of silicotungstic acid loading, the pore size, pore volume and specific surface area of the mesoporous materials are decreased to a certain extent. The reason for the reduction of pore size is probably due to the entry of silicotungstic acid loading components into the channel.

3.3. TEM Image

The modified SBA-15 still presents a six square pass and an ordered mesoporous structure, Figure 2. The loading of silicotungstic acid by impregnation has no significant influence on the skeleton of SBA-15. The pore size of sample is about 4–7 nm, which is reduced to a certain extent compared with pure SBA-15, indicating that the silicotungstic acid has been loaded in the channel.

3.4. FT-IR Analysis

The FT-IR spectra of SBA-15 and SiW_{12}/SBA-15 samples are presented in Figure 3. The FT-IR spectra of both SBA-15 and SiW_{12}/SBA-15 samples are dominated by the asymmetric Si–O–Si stretch at 1110 cm^{-1}. The symmetric stretch occurs at 809 cm^{-1}, while the band at 458 cm^{-1} is assigned to the Si–O–Si bending mode. The band at 971 cm^{-1} can be assigned to the Si–OH vibration generated by the presence of defect sites.

Table II. Characteristics of support and catalysts, specific surface area, SBET (m^2 g^{-1}), pore volume VBJH (cm^3 g^{-1}), pore diameter DBJH (nm).

Loading of silicotungstic acid (wt%)	Surface area (m^2 g^{-1})	Total pore volume (mL g^{-1})	Pore diameter (nm)
0	781.4	0.98	7.0
10	751.2	0.89	6.2
20	661.6	0.86	5.9
30	621.2	0.79	5.4
40	562.8	0.76	5.2
50	483.1	0.74	5.1

The FT-IR absorption peak of SBA-15 lattice water and hydroxyl band is distributed near 3432 and 1600 cm^{-1}. A wider absorption peak near 3432 cm^{-1} belongs to Si–OH outside the SBA-15 skeleton and the stretching vibration peak of adsorbed O–H in water. SiW_{12}/SBA-15 molecular sieves still maintain the characteristic peak of SBA-15 in FT-IR spectrum. It indicates that the skeleton structure of molecular sieve still exists when SBA-15 is modified by silicotungstic acid. The structure of mesoporous molecular sieves SBA-15 loaded by silicotungstic acid was not destroyed. The structure characteristics of Keggin silicotungstic acid are at 1028, 980, 924, and 796 cm^{-1}. Among SiW_{12}/SBA-15 catalyst, the part characteristic absorption peak of silicotungstic acid is obscured by the strong background of SBA-15. The absorption peak can be observed at 980 and 796 cm^{-1}, indicating that silicotungstic acid keeps the basic structure of Keggin.[63]

3.5. RSM Experiment Results

Based on the single-factor experiment, the Response Surface Methodology (RSM) was used to analyze the optimum condition including the loading of silicotungstic acid, the dosage of catalyst, peracetic acid and α-pinene molar ratio, reaction time of the interaction and the optimization condition. The experimental results are shown in Table III. The data were analyzed by employing the

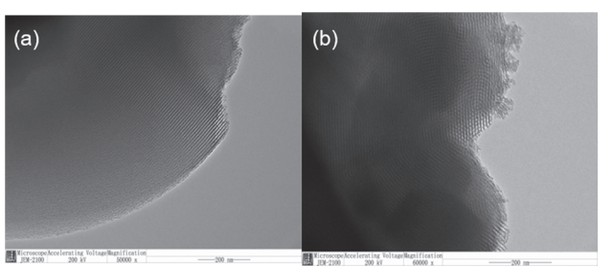

Fig. 2. TEM images of SiW_{12}/SBA-15: (a) Perpendicular to the pore direction, and (b) parallel to the channel direction.

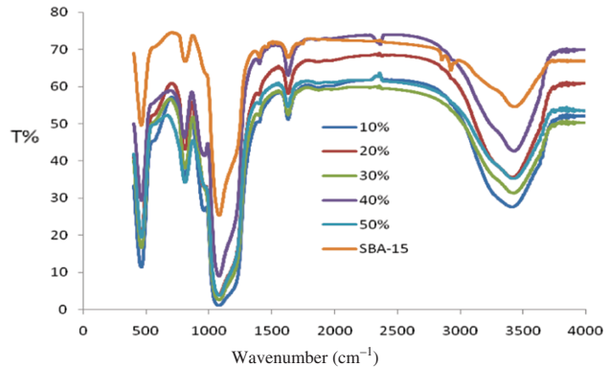

Fig. 3. FT-IR spectra of SBA-15 and different loaded SiW_{12}/SBA-15 samples.

Software Design Expert (version7.0) to develop response surface models. The response and variables are correlated by the following second-order polynomial quadratic equation (3):

$$Y\ (\%) = +94.30 - 4.19 \times X_1 + 1.46 \times X_2 - 0.74 \times X_3 - 0.40 \times X_4 - 1.03 \times X_1 \times X_2 + 0.32 \times X_1 \times X_3 + 1.29 X_1 \times X_4 - 2.51 \times X_2 \times X_3 + 0.20 \times X_2 \times X_4 - 1.30 \times X_3 \times X_4 - 8.23 \times X_1^2 - 2.56 \times X_2^2 - 2.88 \times X_3^2 - 0.17 \times X_4^2 \quad (3)$$

where Y is the response for conversion rate, X_1 is silicotungstic acid loading, X_2 is the dosage of catalyst, X_3 is the molar ratio of peracetic acid to α-pinene, X_4 is the reaction time. The fit of the model is evaluated by coefficient of determination (R^2) and analysis of variance (ANOVA).

Table III. The RSM design and results.

Runs	Loading (%)	Dosage of catalyst (%)	Molar ratio	Reaction time (h)	Conversion rate (%)
1	0	0	−1	1	92.72
2	0	−1	0	1	89.36
3	1	0	1	0	78.82
4	1	0	0	1	82.78
5	0	1	1	0	86.97
6	0	1	−1	0	93.77
7	1	0	−1	0	79.23
8	0	−1	1	0	89.16
9	−1	0	−1	0	88.19
10	0	0	0	0	94.04
11	−1	−1	0	0	85.33
12	0	0	0	0	94.48
13	0	1	0	−1	93.35
14	0	0	1	−1	92.24
15	0	0	0	0	94.24
16	−1	0	0	−1	91.77
17	−1	0	1	0	86.49
18	0	−1	−1	0	85.91
19	−1	1	0	0	90.04
20	0	0	0	0	94.48
21	−1	0	0	1	88.59
22	0	0	0	0	94.27
23	0	−1	0	−1	90.46
24	0	1	0	1	93.05
25	0	0	1	1	88.53
26	1	−1	0	0	78.92
27	1	1	0	0	79.51
28	1	0	0	−1	80.81
29	0	0	−1	−1	91.23

3.6. ANOVA

RSM was applied for successful development, improvements and optimization of the processes. It is the objective of RSM to comprehend the relationships between changes in responses to the adjustment of design variables.[64] So, in the RSM operations algorithm, those variables which have a significant effect on the process are tested simultaneously in a minimum number, according to a suitably selected plan of experiments. In order to determine whether the second-order polynomial model is significant, it is necessary to conduct ANOVA analysis. The data are presented in Table IV. It shows that the second order polynomial model is statistically significant ($P < 0.0001$) and suitable to describe the reaction of peracetic acid and α-pinene. The P-value of 'lack of fit' is 0.2330, which indicates that 'lack of fit' is insignificant relative to the pure error. And the value of the coefficient of determination (R^2) is 0.9988, which can be used to explain 99.88% of total variation in the response, indicating the goodness of the regression model.

Table IV. Statistical analysis of the model.

Source	Sum of squares	Degrees of freedom	Mean square	F value	Prob > F	Significant level
Model	764.05	14	54.57	859.78	<0.0001	***
X_1	211.18	1	211.18	3326.90	<0.0001	***
X_2	25.67	1	25.67	404.36	<0.0001	***
X_3	6.51	1	6.51	102.59	<0.0001	***
X_4	1.94	1	1.94	30.63	<0.0001	***
X_1X_2	4.24	1	4.24	66.85	<0.0001	***
X_1X_3	0.42	1	0.42	6.55	0.027	
X_1X_4	6.63	1	6.63	104.46	<0.0001	***
X_2X_3	25.25	1	25.25	397.80	<0.0001	***
X_2X_4	0.16	1	0.16	2.52	0.1347	
X_3X_4	6.76	1	6.76	106.5	<0.0001	***
X_1^2	413.38	1	413.38	6914.13	<0.0001	***
X_2^2	44.25	1	44.25	668.05	<0.0001	***
X_3^2	56.38	1	56.38	846.47	<0.0001	***
X_4^2	2.57	1	2.57	3.11	0.0998	
Residual	0.89	14	0.063			
Lack of fit	0.75	10	0.075	2.20	0.2330	Not significant
Pure error	0.14	4	0.034			
Cor total	764.94	28				

Note: ***Extremely significant difference ($P < 0.0001$); $P < 0.05$ indicates statistical significance.

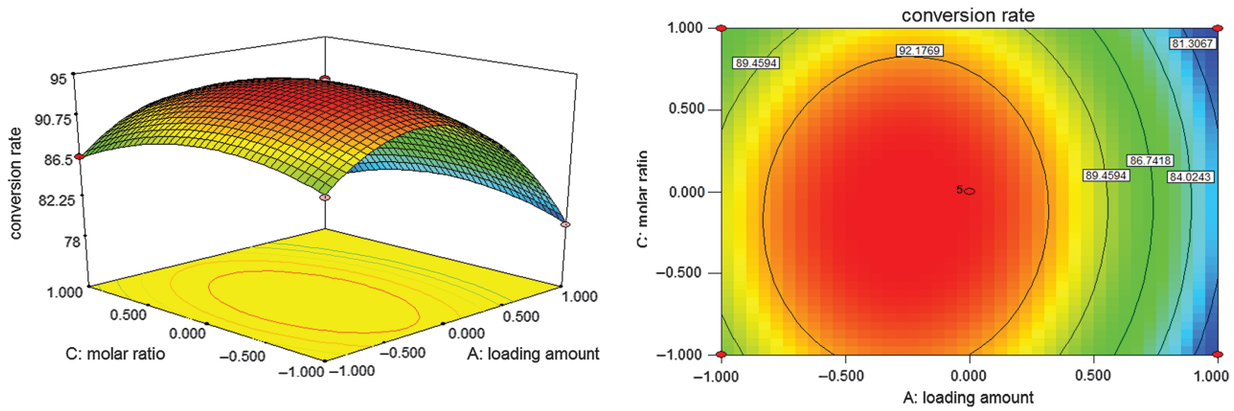

Fig. 4. Response surface plot and contour plot showing the effect of molar ratio and loading amount on the conversion of α-pinene, dosage of catalyst 2% and reaction time 2 h respectively.

From the analysis of the model equation coefficient significance (Table IV), the load (X_1), dosage of catalyst (X_2), molar ratio of peracetic acid to α-pinene (X_3) and reaction time (X_4) all have a significant effect on the conversion rate of α-pinene. The interaction terms (X_1X_2, X_1X_4, X_2X_3, X_3X_4) and the quadratic terms X_1^2, X_2^2 and X_3^2 are significant. However, the interaction terms (X_1X_3, X_2X_4) and the quadratic terms X_4^2 are not significant. These results show that the effects of above various factors on the conversion rate of α-pinene are not a simple linear relationship. The adjusted coefficient of determination (R^2 adj) is 0.9977, which shows the suitability of the model for adequately representing the actual relationship between the responses and the variables.

3.7. Effect of Parameters

The response surfaces and the contour plots generated from the predicted model (Eq. (1) are useful because they provide a visualization of the reaction system for understanding the interactions between two variables and the effects of the experimental variables on the responses.

Figure 4 contains the response surface plot and contour plot showing the effect of molar ratio and loading amount on the 2,3-epoxypinane synthesis at 2% of dosage of catalyst and reaction time of 2 h. The conversion rate of α-pinene increases with the increase in molar ratio up to 1.2 and subsequently starts to decrease. In this case, when peracetic acid is too much, its strong acid may cause the damage to acid binding agent and solvent. Besides, the conversion rate of α-pinene increases with an increase in the loading up to 30% and subsequently starts to decrease. This phenomenon may be due to that with the increase of silicon acid amount, catalyst acidity and activity are increased, but excessive loading will cause the decrease of the pore size of mesoporous SBA-15 by decrease of blocked, aggregation, and reactant contact surface, leading to the decreased catalytic activity.

Figure 5 shows the response surface plot and contour plot showing the effect of reaction time and dosage

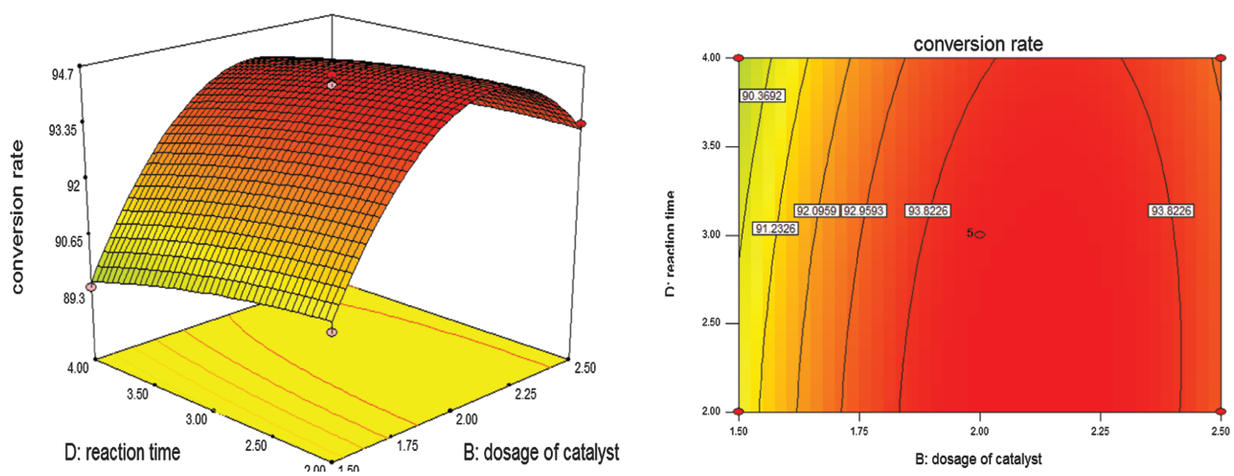

Fig. 5. Response surface plot and contour plot showing the effect of reaction time and dosage of catalyst on the conversion of α-pinene, loading amount 30% and reaction time 2 h respectively.

Table V. Repeating experiment data of SiW_{12}/SBA-15.

Recycling time	Conversion rate %	Selectivity %	Yield %
0	99.07	91.38	90.30
1	93.65	90.38	84.65
2	91.49	90.34	82.65
3	81.65	89.44	73.03
4	80.51	88.10	70.93
5	78.03	87.85	68.55

of catalyst on the 2,3-epoxypinane synthesis at 30% of loading amount and molar ratio 1.2. The conversion of α-pinene increases with an increase in dosage of catalyst up to 2% of the weight of α-pinene, then keeps constant. The conversion of α-pinene increases with an increase in the reaction time up to 3 h then keeps constant.

3.8. Optimization of Reaction Conditions and Model Verification

Based on the discussion above, it is possible to obtain a high yield of 2,3-epoxypinane through searching the optimum point. To validate the predicted results, experiments using the improved formula are performed. The experimental values are found to be reasonably close to the predicted ones, which confirm the validity and adequacy of the predicted models. Under the optimum conditions (22.5% silicotungstic acid loading, 1.8% catalyst dosage, 1.15 peracetic acid and α-pinene molar ratio, the reaction time is 2.5 h), the yield of 2,3-epoxypinane reaches 90.30%.

3.9. Reusability of SiW_{12}/SBA-15

The results of cyclic experiments show that the SiW_{12}/SBA-15 catalyst is stable, and it still has a high catalytic efficiency after 3 times. However, the catalytic activity begins to weaken after fourth times. After fifth time recycling, the catalytic efficiency is still the same as that of pure SBA-15 without loading. The results are summarized in Table V.

4. CONCLUSION

Under acid conditions, the mesoporous molecular sieve SBA-15 was synthesized by hydrothermal synthesis with P123 serving as the templates and $Si(OC_2H_5)_4$ as the silicon source. The SiW_{12}/SBA-15 catalyst prepared by impregnation method was characterized by XRD, TEM, nitrogen adsorption desorption method and FTIR. The SiW_{12}/SBA-15 still presented a six square pass and an ordered mesoporous structure. The loading of silicotungstic acid by impregnation had no significant influences on the skeleton of SBA-15. The pore size of the sample was about 4–7 nm. The silicotungstic acid kept the basic structure of Keggin. The catalysts were used for α-pinene epoxidation. The reaction conditions for epoxidation of α-pinene were optimized using the response surface method and determined as following: the load amount of 30%, the catalyst dosage of 1.8%, the molar ratio of peracetic acid and α-pinene 1.3, and the reaction time is 3 h. The obtained α-pinene conversion rate was 99.07%.

Acknowledgment: This work was financially supported by the 13th Five-Year Plan of National Key R&D Projects of China (No. 2018YFD0600401), National Natural Science Foundation of China (Nos. 31060099, 30700632, 30930074), and Scientific Research Fund Project of Education Department in Yunnan Province, China (No. 2010Z040).

References and Notes

1. B Song, T. Wang, H. Sun, H. Liu, X. Mai, X. Wang, L. Wang, N. Wang, Y. Huang, and Z. Guo, Graphitic carbon nitride (g-C_3N_4) interfacially strengthened carbon fiber epoxy composites. *Compos. Sci. Technol.* 167, 515 **(2018)**.
2. B. Song, T. Wang, L. Wang, H. Liu, X. Mai, X. Wang, N. Wang, Y. Huang, Y. Ma, Y. Lu, E. K. Wujcik, and Z. Guo, Interfacially reinforced carbon fiber/epoxy composite laminates via *in-situ* synthesized graphitic carbon nitride (g-C_3N_4). *Composites B* 158, 259 **(2019)**.
3. B. Kirubasankar, V. Murugadoss, J. Lin, T. Ding, M. Dong, H. Liu, J. Zhang, T. Li, N. Wang, Z. Guo, and S. Angaiaha, *In-situ* grown nickel selenide onto graphene nanohybrid electrodes for high energy density asymmetric supercapacitors. *Nanoscale* 10, 20414 **(2018)**.
4. J. Gu, Y. Li, C. Liang, Y. Tang, L. Tang, Y. Zhang, J. Kong, H. Liu, and Z. Guo, Synchronously improved dielectric and mechanical properties of wave-transparent laminated composites combining with outstanding thermal stability by incorporating iysozyme/POSS functionalized PBO fibers. *J. Mater. Chem. C* 6, 7652 **(2018)**.
5. Z. Wu, H. Cui, L. Chen, D. Jiang, L. Weng, Y. Ma, X. Li, X. Zhang, H. Liu, N. Wang, J. Zhang, Y. Ma, M. Zhang, Y. Huang, and Z. Guo, Interfacially reinforced unsaturated polyester carbon fiber composites with a vinyl ester-carbon nanotubes sizing agent. *Compos. Sci. Technol.* 164, 195 **(2018)**.
6. Y. Sheng, J. Yang, F. Wang, L. Liu, H. Liu, C. Yan, and Z. Guo, Sol–gel synthesized hexagonal boron nitride/titania nanocomposites with enhanced photocatalytic activity. *Appl. Surface Sci.* 465, 154 **(2018)**.
7. H. Shindume, Z. Zhao, N. Wang, H. Liu, A. Umar, J. Zhang, T. Wu, and Z. Guo, Enhanced photocatalytic activity of B,N-codoped TiO_2 by a new molten nitrate process. *J. Nanosci. Nanotechnol.* 19, 839 **(2019)**.
8. W. Deng, T. Kang, H. Liu, J. Zhang, N. Wang, N. Lu, Y. Ma, A. Umar, and Z. Guo, Potassium hydroxide activated and nitrogen doped graphene with enhanced supercapacitive behavior. *Sci. Adv. Mater.* 10, 937 **(2018)**.
9. H. Du, Y. An, Y. Wei, L. Hou, B. Liu, H. Liu, Y. Ma, J. Zhang, N. Wang, A. Umar, and Z. Guo, Nickel powders modified nanocoating strengthened iron plates by surface mechanical attrition alloy and heat treatment. *Sci. Adv. Mater.* 10, 1063 **(2018)**.
10. P. Zhang, T. Ge, H. Yang, S. Lin, Y. Cao, C. Zhao, H. Liu, A. Umar, and Z. Guo, Antifouling of titania nanostructures in real maritime conditions. *Sci. Adv. Mater.* 10, 1216 **(2018)**.
11. C. Wang, B. Mo, Z. He, Q. Shao, D. Pan, E. Wujick, J. Guo, X. Xie, X. Xie, and Z. Guo, Crosslinked norbornene copolymer anion exchange membrane for fuel cells. *J. Membrane Sci.* 556, 118 **(2018)**.

12. K. Gong, Q. Hu, Y. Xiao, X. Cheng, H. Liu, N. Wang, B. Qiu, and Z. Guo, Triple layered core–shell ZVI@carbon@polyaniline composites enhanced electron utilization in Cr(VI) reduction. *J. Mater. Chem. A* 6, 11119 **(2018)**.

13. J. Huang, Y. Li, Y. Cao, F. Peng, Y. Cao, Q. Shao, H. Liu, and Z. Guo, Hexavalent chromium removal over magnetic carbon nanoadsorbent: Synergistic effect of fluorine and nitrogen co-doping. *J. Mater. Chem. A* 6, 13062 **(2018)**.

14. K. Gong, S. Guo, Y. Zhao, Q. Hu, H. Liu, D. Sun, M. Li, B. Qiu, and Z. Guo, Bacteria cell templated porous polyaniline facilitated detoxification and recovery of hexavalent chromium. *J. Mater. Chem. A* 6, 16824 **(2018)**.

15. K. Sun, R. Fan, X. Zhang, Z. Zhang, Z. Shi, N. Wang, P. Xie, Z. Wang, G. Fan, H. Liu, C. Liu, T. Li, C. Yan, and Z. Guo, An overview of metamaterials and their achievements in wireless power transfer. *J. Mater. Chem. C* 6, 2925 **(2018)**.

16. C. Wang, B. Mo, Z. He, C. X. Zhao, L. Zhang, Q. Shao, X. Guo, E. Wujcik, and Z. Guo, Hydroxide ions transportation in polynorbornene anion exchange membrane. *Polymer* 138, 363 **(2018)**.

17. P. Xie, Z. Wang, Z. Zhang, R. Fan, C. Cheng, H. Liu, Y. Liu, T. Li, C. Yan, N. Wang, and Z. Guo, Silica microspheres templated self-assembly of three-dimensional carbon network with stable radio-frequency negative permittivity and low dielectric loss. *J. Mater. Chem. C* 6, 5239 **(2018)**.

18. X. Wang, X. Liu, H. Yuan, H. Liu, C. Liu, T. Li, C. Yan, X. Yan, C. Shen, and Z. Guo, Non-covalently functionalized graphene strengthened poly(vinyl alcohol). *Mater. Design* 139, 372 **(2018)**.

19. M. Zhao, L. Meng, L. Ma, X. Yang, Y. Huang, J. Ryu, A. Shankar, T. Li, C. Yan, and Z. Guo, Layer-by-layer grafting CNTs onto carbon fibers surface for enhancing the interfacial properties of epoxy resin composites. *Compos. Sci. Technol*. 154, 28 **(2018)**.

20. H. Liu, W. Huang, X. Yang, K. Dai, G. Zheng, C. Liu, C. Shen, X. Yan, J. Guo, and Z. Guo, Organic vapor sensing behaviors of conductive thermoplastic polyurethane-graphene nanocomposites. *J. Mater. Chem. C* 4, 4459 **(2018)**.

21. K. Zhang, G. Li, L. Feng, N. Wang, J. Guo, K. Sun, K. Yu, J. Zeng, T. Li, Z. Guo, and M. Wang, Ultralow percolation threshold and enhanced electromagnetic interference shielding in poly(L-lactide)/multi-walled carbon nanotubes nanocomposites with electrically conductive segregated networks. *J. Mater. Chem. C* 5, 9359 **(2017)**.

22. Z. Wang, H. Zhu, N. Cao, R. Du, Y. Liu, and G. Zhao, Superhydrophobic surfaces with excellent abrasion resistance based on benzoxazine/mesoporous SiO_2. *Mater. Lett.* 186, 274 **(2017)**.

23. C. Wang, Z. He, X. Xie, X. Mai, Y. Li, T. Li, M. Zhao, C. Yan, H. Liu, E. Wujcik, and Z. Guo, Controllable cross-linking anion exchange membranes with excellent mechanical and thermal properties. *Macromol. Mater. Eng.* 3, 1700462 **(2018)**.

24. Y. Zhang, M. Zhao, J. Zhang, Q. Shao, J. Li, H. Li, B. Lin, M. Yu, S. Chen, and Z. Guo, Excellent corrosion protection performance of epoxy composite coatings filled with silane functionalized silicon nitride. *J. Polymer Research* 25, 130 **(2018)**.

25. L. Wang, H. Qiu, C. Liang, P. Song, Y. Han, Y. Han, J. Gu, J. Kong, D. Pan, and Z. Guo, Electromagnetic interference shielding MWCNT-Fe_3O_4@Ag/epoxy nanocomposites with satisfactory thermal conductivity and high thermal stability. *Carbon* 141, 506 **(2019)**.

26. Z. Zhao, R. Misra, P. Bai, J. Gao, Y. Li, R. Guan, and Z. Guo, Novel process of coating Al on graphene involving organic aluminum accompanying microstructure evolution. *Mater. Lett.* 232, 202 **(2018)**.

27. Y. He, S. Yang, H. Liu, Q. Shao, Q. Chen, C. Lu, Y. Jiang, and Z. Guo, Reinforced carbon fiber laminates with oriented carbon nanotube epoxy nanocomposites: Magnetic field assisted alignment and cryogenic temperature mechanical properties. *J. Colloid Interf. Sci.* 517, 40 **(2018)**.

28. Z. Wu, S. Gao, L. Chen, D. Jiang, Q. Shao, B. Zhang, Z. Zhai, C. Wang, M. Zhao, Y. Ma, X. Zhang, L. Weng, M. Zhang, and Z. Guo, Electrically insulated epoxy nanocomposites reinforced with synergistic core–shell SiO_2@MWCNTs and montmorillonite bifillers. *Macromol. Chem. Phys*. 218, 1700357 **(2017)**.

29. T. Su, Q. Shao, Z. Qin, Z. Guo, and Z. Wu, Role of interfaces in two-dimensional photocatalyst for water splitting. *ACS Catal.* 8, 2253 **(2018)**.

30. C. Wang, V. Murugadoss, J. Kong, Z. He, X. Mai, Q. Shao, Y. Chen, L. Guo, C. Liu, S. Angaiah, and Z. Guo, Overview of carbon nanostructures and nanocomposites for electromagnetic wave shielding. *Carbon* 140, 696 **(2018)**.

31. L. Zhang, W. Yu, C. Han, J. Guo, Q. Zhang, H. Xie, Q. Shao, Z. Sun, and Z. Guo, Large scaled synthesis of heterostructured electrospun TiO_2/SnO_2 nanofibers with an enhanced photocatalytic activity. *J. Electrochem. Soc.* 164, H651 **(2017)**.

32. B. Song, T. Wang, H. Sun, Q. Shao, J. Zhao, K. Song, L. Hao, L. Wang, and Z. Guo, Two-step hydrothermally synthesized carbon nanodots/WO_3 photocatalysts with enhanced photocatalytic performance. *Dalton Trans.* 46, 15769 **(2017)**.

33. C. Wang, M. Zhao, J. Li, J. Yu, S. Sun, S. Ge, X. Guo, F. Xie, B. Jiang, E. Wujcik, Y. Huang, N. Wang, and Z. Guo, Silver nanoparticles/graphene oxide decorated carbon fiber synergistic reinforcement in epoxy-based composites. *Polymer* 131, 263 **(2017)**.

34. J. Zhao, L. Wu, C. Zhan, Q. Shao, Z. Guo, and L. Zhang, Overview of polymer nanocomposites: Computer simulation understanding of physical properties. *Polymer* 133, 272 **(2017)**.

35. P. Zhou, S. Wang, C. Tao, X. Guo, L. Hao, Q. Shao, L. Liu, Y. Wang, W. Chu, B. Wang, S. Luo, and Z. Guo, PAA/alumina composites prepared with different molecular weight polymers and utilized as support for nickel-based catalyst. *Adv. Polym. Technol.* 37, 2325 **(2018)**.

36. Y. Wang, P. Zhou, S. Luo, X. Liao, B. Wang, Q. Shao, X. Guo, and Z. Guo, Controllable synthesis of monolayer poly(acrylic acid) on channel surface of mesoporous alumina for Pb(II) adsorption. *Langmuir* 34, 7859 **(2018)**.

37. Z. Hu, D. Zhang, F. Lu, W. Yuan, X. Xu, Q. Zhang, H. Liu, Q. Shao, Z. Guo, and Y. Huang, Multistimuli-responsive intrinsic self-healing epoxy resin constructed by host-guest interactions. *Macromolecules* 51, 5294 **(2018)**.

38. Z. Zhao, P. Bai, R. Guan, V. Murugadoss, H. Liu, X. Wang, and Z. Guo, Microstructural evolution and mechanical strengthening mechanism of Mg-3Sn-1Mn-1La alloy after heat treatments. *Mater. Sci. Eng. A* 734, 200 **(2018)**.

39. W. Du, X. Wang, J. Zhan, X. Sun, L. Kang, F. Jiang, X. Zhang, Q. Shao, M. Dong, H. Liu, V. Murugadoss, and Z. Guo, Biological cell template synthesis of nitrogen-doped porous hollow carbon spheres/MnO_2 composites for high-performance asymmetric supercapacitors. *Electrochim. Acta* 296, 907 **(2019)**.

40. A. Sayari, Synthetic self-assembled materials: Principles and practice. *Chem. Mater*. 8, 1840 **(1996)**.

41. F. J. Trindade, G. J. T. Fernandes, A. S. Araújo, V. J. Fernandes Jr., B. P. G. Silva, R. Y. Nagayasu, M. J. Politi, F. L. Castro, and S. Brochsztain, Covalent attachment of 3,4,9,10-perylenediimides onto the walls of mesoporous molecular sieves MCM-41 and SBA-15. *Micropor. Mescpor. Mat*. 113, 463 **(2008)**.

42. J. Ma, L. S. Qiang, J. F. Wang, X. B. Tang, and D. Y. Tang, Effect of different synthesis methods on the structural and catalytic performance of SBA-15 modified by aluminum. *J. Porous. Mat.* 18, 607 **(2011)**.

43. Z. Luan, M. Hartmann, D. Maes, W. Zhao, L. Zhou, and L. Kevan, Alumination and ion exchange of mesoporous SBA-15 molecular sieves. *Chem. Mater*. 11, 1621 **(1999)**.

44. Z. Luan, E. M. Maes, P. A. W. VanderHeide, D. Zhao, R. S. Czernuszewicz, and L. Kevan, Incorporation of titanium into mesoporous silica molecular sieve SBA-15. *Chem. Mater.* 11, 3680 **(1999)**.

45. S. Y. Chen, T. Mochizuki, Y. Abe, M. Toba, Y. Yoshimura, P. Somwongsa, and S. Lao-Ubol, Carbonaceous Ti-incorporated

ARTICLE

SBA-15 with enhanced activity and durability for high-quality biodiesel production: Synthesis and utilization of the P123 template as carbon source. *Appl. Catal. B-Environ.* 181, 800 **(2016)**.

46. P. Shah, A. V. Ramaswamy, K. Lazar, and V. Ramaswamy, Synthesis and characterization of tin oxide-modified mesoporous SBA-15 molecular sieves and catalytic activity in trans-esterification reaction. *Appl. Catal. A-Gen*. 273, 239 **(2004)**.

47. G. J. Wang, S. Zhang, Y. H. Huang, F. F. Kang, Z. X. Yang, and Y. J. Gu, Styrene epoxidation over V-SBA-15 with alkaline-earth metal ion promotion under photo-assisted conditions. *Appl. Catal. A-Gen.* 413–414, 52 **(2012)**.

48. Q. Y. Liu, W. L. Wu, J. Wang, X. Q. Ren, and Y. R. Wang, Characterization of 12-tungstophosphoric acid impregnated on mesoporous silica SBA-15 and its catalytic performance in isopropylation of naphthalene with isopropanol. *Micropor. Mescpor. Mat.* 76, 51 **(2004)**.

49. N. Y. He, C. S. Woo, H. G. Kim, and H. I. Lee, Catalytic formation of acetic anhydride over tungstophosphoric acid modified SBA-15 mesoporous materials. *Appl. Catal. A-Gen.* 281, 167 **(2005)**.

50. B. S. Lane and K. Burgess, Metal-catalyzed epoxidations of alkenes with hydrogen peroxide. *Chem. Rev.* 103, 2457 **(2003)**.

51. Q. H. Xia, H. Q. Ge, C. P. Ye, Z. M. Liu, and K. X. Su, Advances in homogeneous and heterogeneous catalytic asymmetric epoxidation. *Chem. Rev.* 105, 1603 **(2005)**.

52. I. Schmidt, A. Krogh, K. Wienberg, A. Carlsson, M. Brorson, and C. J. H. Jacobsen, Catalytic epoxidation of alkenes with hydrogen peroxide over first mesoporous titanium-containing zeolite. *Chem. Commun*. 21, 2157 **(2000)**.

53. G. Grigoropoulou, J. H. Clark, and J. A. Elings, Recent developments on the epoxidation of alkenes using hydrogen peroxide as oxidant. *Green Chem.* 5, 1 **(2003)**.

54. D. Y. Zhao, J. L. Feng, Q. S. Huo, N. Melosh, G. H. Fredrickson, B. F. Chmelka, and G. D. Stucky, Triblock copolymer syntheses of mesoporous silica with periodic 50 to 300 angstrom pores. *Science* 279, 548 **(1998)**.

55. M. Kruk, M. Jaroniec, C. H. Ko, and R. Ryoo, Characterization of the porous structure of SBA-15. *Chem. Mater*. 12, 1961 **(2000)**.

56. B. P. Wu, Z. W. Tong, and X. D. Yuan, Synthesis, characterization and catalytic application of mesoporous molecular sieves SBA-15 functionalized with phosphoric acid. *J. Porous. Mat*. 19, 641 **(2012)**.

57. S. J. Gregg and K. S. Sing, Adsorption, Surface Area and Porosity, Academic Press, London **(1982)**.

58. J. J. Zhu, T. Wang, X. L. Xu, P. Xiao, and J. L. Li, Pt nanoparticles supported on SBA-15: Synthesis, characterization and applications in heterogeneous catalysis. *Appl. Catal. B-Environ.* 130–131, 197 **(2013)**.

59. Y. Q. Zhang, S. J. Wang, J. W. Wang, L. L. Lou, C. Zhang, and S. X. Liu, Synthesis and characterization of Zr-SBA-15 supported tungsten oxide as a new mesoporous solid acid. *Solid State Sci.* 11, 1412 **(2009)**.

60. X. L. Sheng, J. Kong, Y. M. Zhou, Y. W. Zhang, Z. W. Zhang, and S. J. Zhou, Direct synthesis, characterization and catalytic application of SBA-15 mesoporou. silica with heteropolyacid incorporated into their framework. *Micropor. Mesopor. Mat.* 187, 7 **(2014)**.

61. G. S. Kumar, M. Vishnuvarthan, M. Palanichamy, and V. Murugesan, SBA-15 supported HPW Effective catalytic performance in the alkylation of phenol. *J. Mol. Catal. A-Chem.* 260, 49 **(2006)**.

62. F. S. Xiao, Hydrothermally stable and catalytically active ordered mesoporous materials assembled from preformed zeolite nanoclusters. *Catal. Surv. Asia* 8, 151 **(2004)**.

63. B. C. Gagea, Y. Lorgouilloux, Y. Altintas, P. A. Jacobs, and J. A. Martens, Bifunctional conversion of *n*-decane over HPW heteropoly acid incorporated into SBA-15 during synthesis. *J. Catal.* 265, 99 **(2009)**.

64. D. C. Montgomery, Design and Analysis of Experiments, Wiley, New York **(2001)**.

ARTICLE